Nuclear Inst. and Methods in Physics Research, A 1045 (2023) 167545

Contents lists available at ScienceDirect

Nuclear Inst. and Methods in Physics Research, A

journal homepage: www.elsevier.com/locate/nima

Real-time digital signal processing implementation for in-beam PET of radiotherapy imaging in HIMM

J.W. Yan [a], Genyuan Liang [a,b], Jin-Da Chen [a], Chang-Xin Wang [a], Xiu-Ling Zhang [a], Min-Chi Hu [a,b], Cheng-Ming Du [c], Chang-Xu Pei [d], Qian-Shun She [a], Hong-yun Zhao [a], Yi Qian [a], Hong Su [a], J. Kong [a,*]

[a] Institute of Modern Physics, Chinese Academy of Sciences, Lanzhou 730000, China
[b] School of Nuclear Science and Technology, University of Chinese Academy of Sciences, Beijing 100049, China
[c] School of Electronic Engineering, Chaohu University, Hefei 238000, China
[d] School of Nuclear Science and Technology, Lanzhou University, Lanzhou 730000, China

ARTICLE INFO

Keywords:
Digital signal processing
Field-programmable gate array (FPGA)
In-beam positron emission tomography (ibPET)
In-beam monitoring

ABSTRACT

The in-beam positron emission tomography (ibPET) is dedicated to radiotherapy imaging of the heavy-ion medical machine (HIMM), which requires precise online measurement, as well as real-time signal processing capability of the electronics. In this paper, we present the implementation of real-time digital signal processing in the data acquisition unit (DAQU) for an ibPET system based on the photomultiplier tube (PMT) readout of lutetium-yttrium oxyorthosilicate (LYSO) scintillator crystals. We have designed 10-channel customized signal processing circuit on a high-performance FPGA, which supports 3 working modes (single event processing mode, self-calibration mode and raw ADC data mode), position calculation, crystal locating, event sorting, and etc. Moreover, the implementation of real-time corrections is capable of dealing with photon peak correction to 511 keV and crystal ID-based time correction. The implemented real-time ibPET system can achieve 46% data compression and beyond 1,000,000 events/sec/channel signal processing capabilities. A series of initial tests is conducted, and the results indicate that this design meets the application requirement on online processing.

1. Introduction

The number of centers where particle therapy is employed for cancer treatment is increasing worldwide [1], as heavy charged particles have a more selective deposition of energy in depth and an increased biological effectiveness [2,3]. Therefore, the real-time monitoring of beam spatial and dose distribution during the treatment, which can ensure the safety and accuracy of the treatment plan, becomes the hotspot in the fields of radiology and nuclear medicine. The GSI group uses the first to use the so-called 'in-beam positron emission tomography (In-beam PET)' [4–6] monitoring technique in the clinical routine. An In-beam PET is developed for monitoring the irradiation dose and position accurately delivered to patient through the detection of annihilation events generated at the irradiation area during ion beam therapy, and completing the color-scale image reconstruction for treatment validation [7]. Some other research teams have developed specifically tailored system geometries for small-scoped clinical imaging applications, including dedicated detectors and readout electronic systems, verifying the feasibility and clinical value of ibPET [8–10].

The first generation heavy-ion medical machine (HIMM) [11,12] has been constructed for cancer therapy at the Wuwei, Gansu, treatment center for clinical application. To improve the performance of the domestic HIMM industrialization device, a dedicated ibPET will be mounted on the beam line in the upgraded HIMM for in vivo and non-invasive monitoring. However, there is still lack of solutions to integrate a commercial PET into a treatment center today [13,14], thus the dedicated detectors need to be developed. A dual planar geometry, which allows the beam to pass through the patient without hitting the detectors of the PET scanner, is particularly convenient for ibPET [5,6]. Such systems have challenges in accurate reconstruction, where images have to be generated under high count rate and within a short time to allow feedback. Therefore, its readout electronics is required to have the capability of real-time position, time and energy measurement with high-resolution [15–17]. In the paper, a design implementation of real-time digital signal processing is presented, which is developed for the Data Acquisition Unit (DAQU) of ibPET. The ibPET system architecture, firmware implemented in FPGA, real-time digital signal processing, correction algorithm, and performances evaluation are described in the following sections.

* Corresponding author.
E-mail address: kongjie@impcas.ac.cn (J. Kong).

https://doi.org/10.1016/j.nima.2022.167545
Received 17 May 2022; Received in revised form 26 September 2022; Accepted 1 October 2022
Available online 14 October 2022

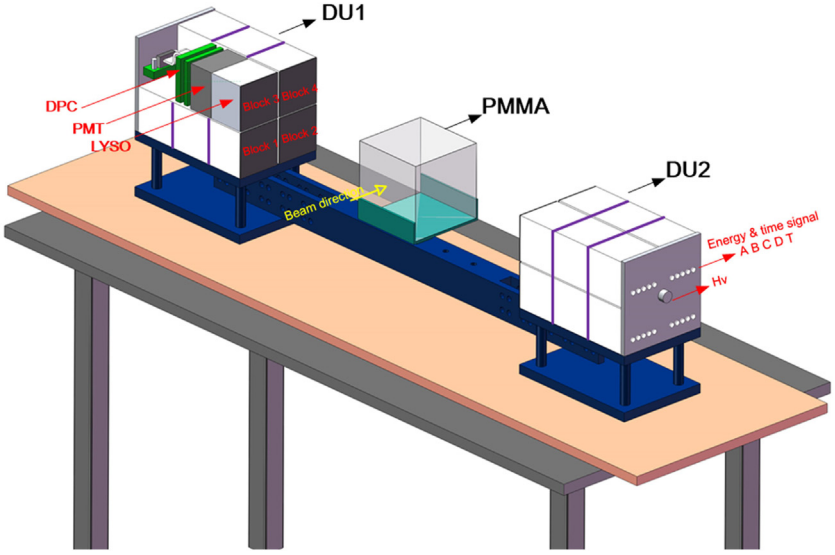

Fig. 1. 3-D structural diagram of the Dual-Head Planar-Type detector array.

2. The In-beam PET system

The prototype of in-beam PET system consists of two parts. The detector unit called Dual-Head Planar-Type detector array and a readout electronic system. Fig. 1 shows Dual-Head Planar-Type detector array consists of eight detector blocks in the prototype system. These detector blocks are divided into two groups. Each group is arranged into a detector array of 2 × 2 blocks, as one detection head of the detector unit. These two detection heads are located oppositely at both sides of beam line along with the direction of beam. Each detector block includes 22 × 22 LYSO [18,19] pixel elements (2 mm × 2 mm × 15 mm) and is read out by a Hamamatsu H8500C [20] PMT and a bridged circuit named as Discretized Positioning Circuit (DPC) [21]. The DPC reduces the number of PMT signals from 64 to only 4 per block to measure the energy. The last dynode of PMT is used for timing.

The electronics system includes the data acquisition unit (DAQU), central processing module (CPM), and clock & synchronize unit (CSU). Signals from the detectors are first fed to the DAQUs. Each DAQU deals with a pair of detector blocks, as shown in Fig. 2. A more detailed description of the hardware circuit designed for DAQU can be found in [22]. We further optimized and developed a real-time digital signal processing features. Beyond the raw ADC data mode, single event processing mode and self-calibration mode were added. The valid information (i.e., position, time, particle energy, etc.) for each event are abstracted and arranged into data frames in the DAQUs, and then transferred to a CPM through a high-speed optical fiber link. CPM is employed to sort the data frames into chronological order according to the timestamp of each event, so as to identify the coincidence events efficiently [23]. Then, event data are interfaced to the host PC through PCIe interface for 3D image reconstruction. Meanwhile, a CSU provide clock and synchronization signals to all DAQU to form a synchronized readout system.

3. Design of DAQU event processing logic

There are three processing modes implemented on a high performance FPGA. The single event processing mode is used to calculate position, time, and energy information. This mode is used for the common imaging processing in the ibPET system. The self calibration mode obtains the crystal look-up table (CLUT) and the normalization LUT (NLUT) for system calibration. The raw ADC data mode is reserved for system diagnosis (see Fig. 3).

3.1. Single event processing mode

In actual application, the single event processing mode calculates the reaction crystal address (i.e., position information), energy and time measurement result of each event. The detailed signal processing block diagram of this mode is reproduced in Fig. 4. The first processing step is to calculate the 'area' data [marked as $E_A \sim E_D$] of each of the corner signals and the four 'area' values are summed together to create an E_{sum} according to Eq. (1). All of this data has a bit width of 16 bits and would be extracted as input data words from the rising edge of the time signal. To obtain the position results, the raw position of each event in the X- and Y-directions [marked as position (X, Y)] with a bit width of 16 bits [8 bits for X and 8 bits for Y] was calculated, according to Eqs. (2) and (3).

$$E = E_A + E_B + E_C + E_D \tag{1}$$

$$X = 128 \times 2 \times \left(\frac{E_A + E_B}{E_A + E_B + E_C + E_D}\right) \tag{2}$$

$$Y = 128 \times 2 \times \left(\frac{E_A + E_C}{E_A + E_B + E_C + E_D}\right) \tag{3}$$

Using the raw position (Y, X) as the CLUT RAM read address, we can finally get the interaction crystal location called the ID number. Event processing in this mode has been divided into two main stages in pipeline: energy calibration and time correction. The pipelining design maximizes the efficiency of data processing and allows for the reduction of the processing logic time-consuming. When the mismatches due to crystals, PMTs, and the electronics are taken into account, the coefficients vary with different ID numbers. These IDs and coefficients are established through the result of the self-calibration mode and are stored in the CLUT and NLUT RAM, respectively. As for the energy calibration, E_{sum} is converted to the energy with the unit of kiloelectronvolts around 511 keV marked as E_{nor}, by multiplying a coefficient corresponding to the ID number. Meanwhile, an adjustable range filtering window is implemented to filter the Compton events. After that, the corrected values (E_{nor}) of the energy are filtered and sent to the data packaging. Due to the delay mismatch caused by the crystals, PMTs, and electronics, the time [marked as T_p] from the output of the TDC is also required for correction. The time correction uses the calibration delay offset value from crystal-by-crystal to correct the timestamp value. The delay offset from the corresponding time LUT reads out according to the ID number, and then by subtracting this offset from T_p. After then, the results are also transferred to the data packaging.

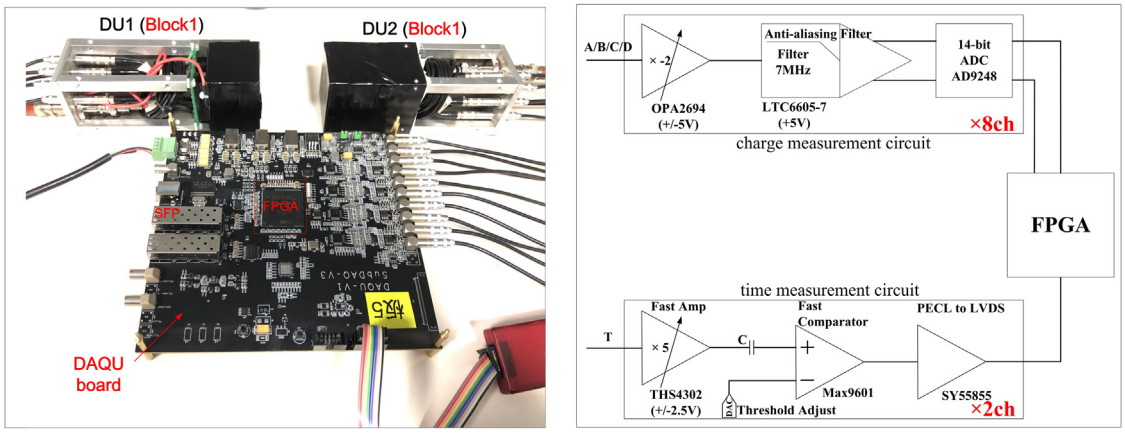

Fig. 2. A picture of one DAQU connection with a pair of detector blocks and the block diagram of the DAQU.

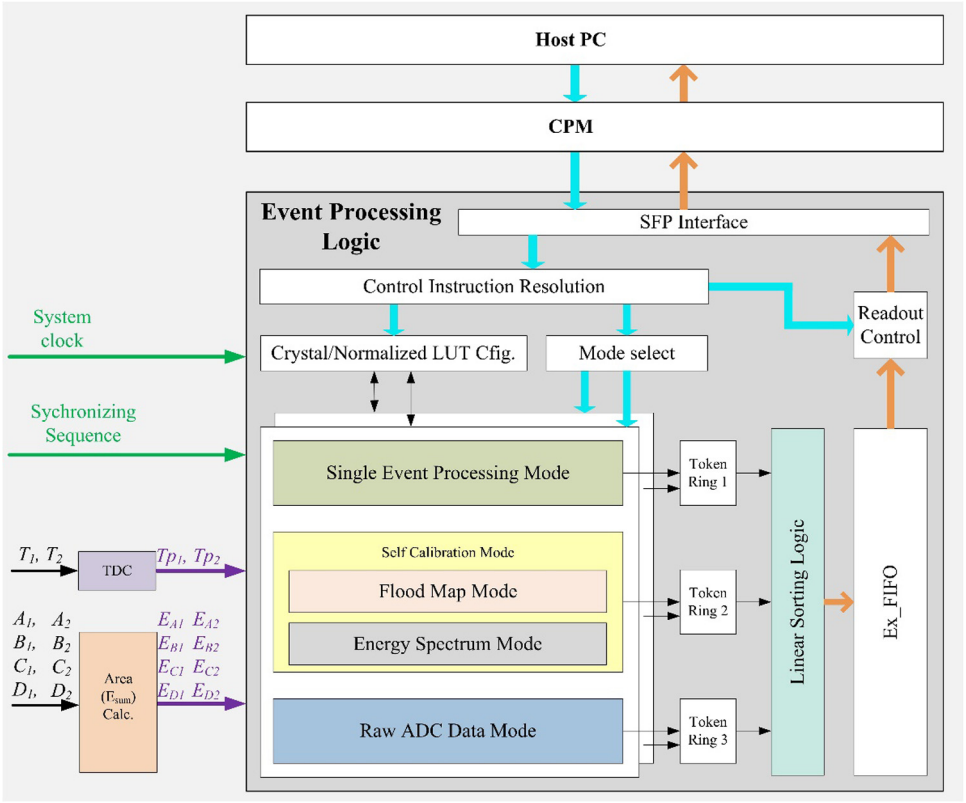

Fig. 3. Simplified scheme of the firmware architecture of the DAQU's FPGA. It shows the structure of the event processing logic, which can work in single event processing mode, self-calibration mode, and raw ADC data mode.

The data packaging module takes the collected final position, time, and energy results and combines them to ten 16 bit fixed packets as one frame format, as shown in Table 1, and then temporarily holds them in a FIFO. Meanwhile, a token ring structure is applied to readout data from FIFO to avoid overflow. Moreover, to meet the maximum required data rate of the logic is 1,000,000 events/s, the token ring takes only ten clock cycles (i.e., 100 ns) to transfer the data frame in the FIFO to the last processing step which is the linear sorting logic module [24]. This guarantees that the data frames of events are outputted in chronological order and stored in the Ex_FIFO. The data output from the Ex_FIFO is transferred to the CPM for further data package sorting as mentioned in [23]. This kind of real-time data manipulation and pipelining designed as mentioned above can alleviate off-line processing without affecting dead-time or data throughput.

3.2. Self-calibration mode

To obtain the location statistic graph of the photons hitting the detector crystal, self-calibration mode is used to count the number of hits on each crystal lattice point by integrating the functions implemented in the previous software. By using this mode, the statistical value of each crystal lattice point being hit will be directly outputted by the hardware. The corresponding coordinates of X and Y are calculated using the formula (1) and (2).

The A, B, C and D represent the charge signals of the four channels of a detector block, X and Y represent the coordinate values in the X- and Y-direction of the corresponding crystal strip. When under the self-calibration mode, the four charge signals are calculated to obtain the 'area' information, respectively, as shown in Fig. 5. Then each signal is marked for channel sorting, through the formula conversion

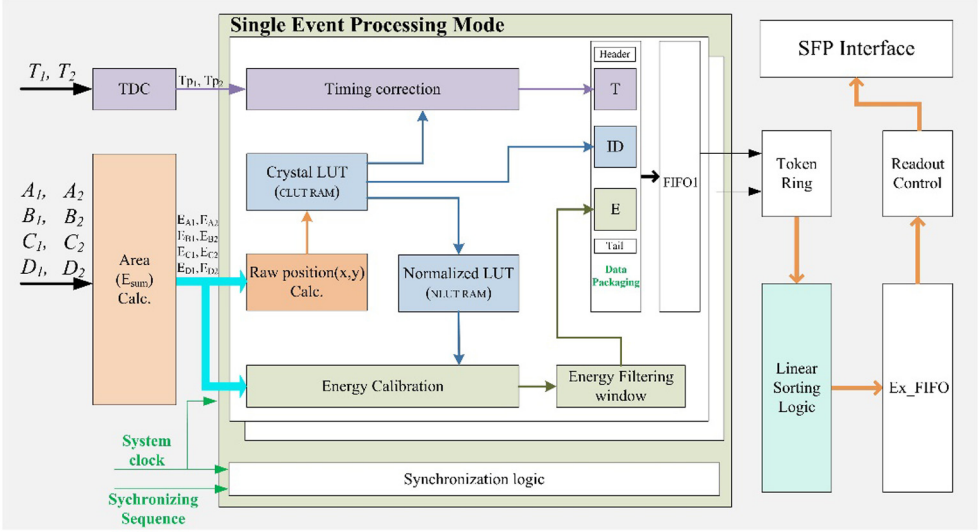

Fig. 4. Simplified the block diagram of the single event processing mode. Calculate the reaction crystal address (i.e., position information), energy, and time measurement result of each event.

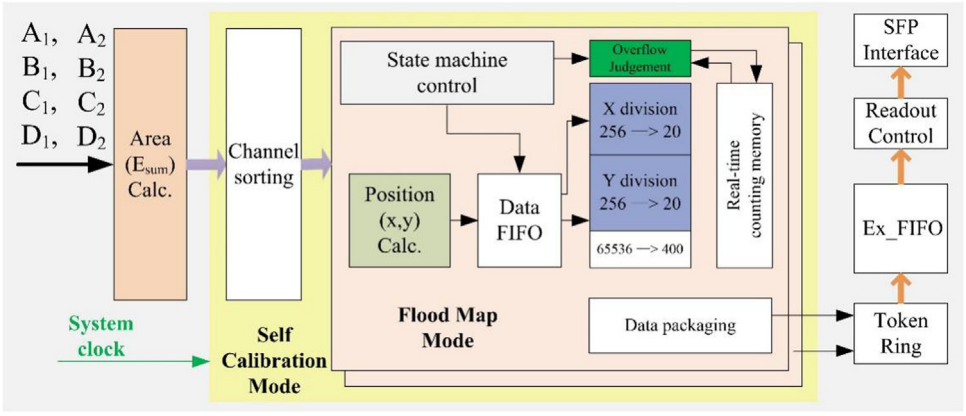

Fig. 5. Simplified block diagram of the self-calibration mode.

Table 1
Output data format of single event processing mode.

31 16	15 0
Heaer (16 bit)	Channel (16 bit)
coarse timestamp (32 bit)	
coarse timestamp (26 bit)	fine time (6 bit)
ID (16 bit)	E_{nor} (16 bit)
reserved (16 bit)	Tail (16 bit)

relationship, and the energy values [marked $E_A/E_B/E_C/E_D$] obtained by the energy calculation module are used to calculate the position information.

The value of calculated coordinates X and Y are 8 bits in width respectively and then are spliced together to form a 16 bit word that is stored in the FIFO. If the FIFO is not empty, the data stored in FIFO is divided from 65 536 areas into 400 intervals by doing a compression of 256 to 40 in the X- and Y-directions respectively. The corresponding position coordinate point is converted to an interval range of 0 to 256, and is mapped to the range of 0 to 20 in the X and Y directions in the digital process unit, respectively, to correspond to the range of $20 \times 20 = 400$ crystal strips of the detectors. The statistics of the hits corresponding to the number of points of all crystal strips are stored in a one-dimensional real-time counting memory. Once the count value of one of the crystal lattices overflows, the corresponding count value of all points will be output to be data packing module for further data transmission. At this point, the coordinates of an event have been calibrated in the DAQU unit.

3.3. Raw ADC data mode

The function of raw ADC data mode is to directly transmit the collected energy and time information from each channel to the data packaging and upload them to the upper computer without any processing. In current application all 8 channels are equipped with 14 bit ADCs, running at 50 MHz. The output data frame contains 33 sampling points in this mode. After uploading the data packet, user can process

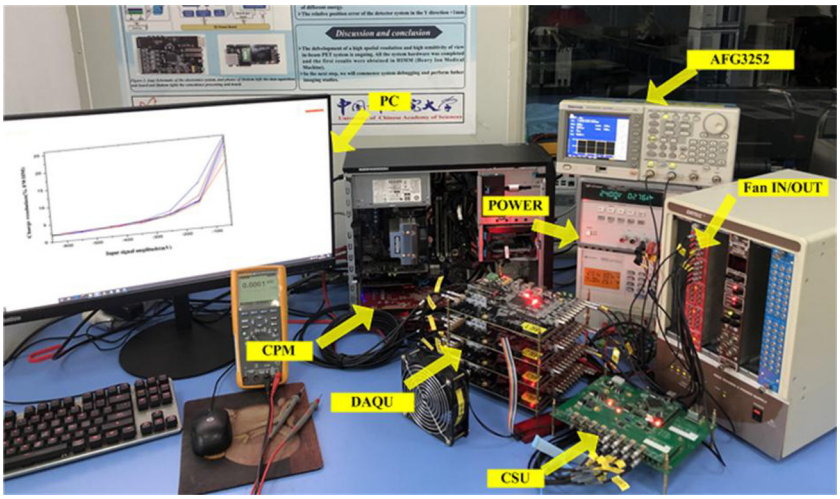

Fig. 6. A system under test was set up in the laboratory. In the picture four DAQU boards have been connected. The current acquisition implementation is already capable of handling up to two DUs with four detector blocks.

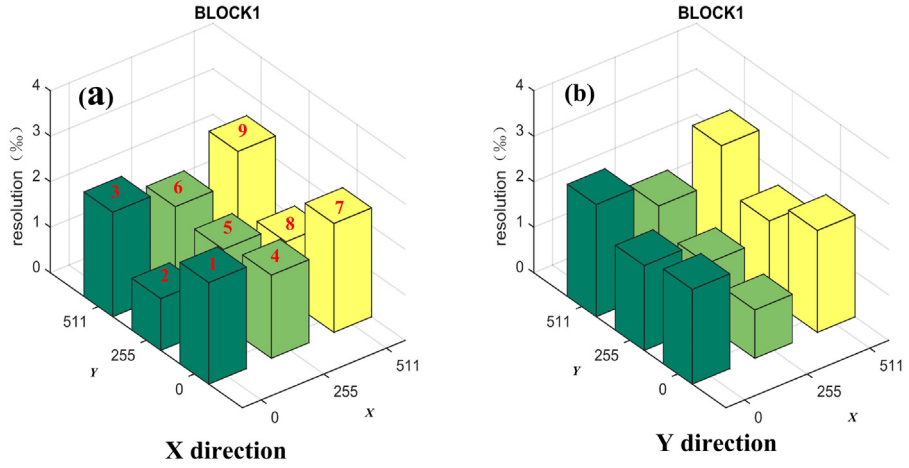

Fig. 7. X- and Y- directions position resolution test results of block 1 in DU (nine positions about the center, four corners, and the center of the four sides).

off-line based on software programming on the host PC, including position, time and energy resolution calculations. To verify the effectiveness of the newly implemented in-time processing logic, the results of real-time data processing performed by the hardware can be compared with off-line results.

3.4. Data compression and transmission

To prove that our in-beam PET is a real-time system, the next unavoidable issue is the data compression rate. Generally, the actual data compression rate under a given digital signal processing mode is dominated by the effective data words in the data frame. Based on implemented data frame in our system, the data compression rate can be evaluated by two technical methods single event processing mode and raw ADC data mode. As mentioned in Section 3.1, the largest data frame consumption under single event processing mode is 20 bytes, while the valid data word is 12 bytes, which includes timestamp, ID and E_{nor}. This allows for easy data reduction on the DAQU board. Regarding the raw ADC data mode, to transmit the collected pulse event as completely as possible, the valid data word in the data frame contains the timestamp, the amplitude of 33 sampling points, and a total of 272 bytes [22]. Using the single event processing mode to calculate effective data words in real-time, we can significantly reduce the data consumption in transmission with a data compression rate of 96%. Meanwhile, in real-time processing with the energy filtering window of [450,600] keV, where the data compression rate measured with a ^{22}Na point source was found to be 49%. The above real-time processing methods can achieve up to 46% compression rate in total thus, significantly improving in-beam PET real-time performance.

Considering that we plan to will expand the system to 36 detector units in the future, the transmission data capacity will be doubled. In real application, data transmission is based on optical fiber links. To combine the data streams of several DAQU modules, fiber links of up to eight boards can be connected to a CPM module.

4. Testing results and comparison

4.1. Performance test results of the DAQU

The performances of the DAQU module include position, time, and energy measurement resolution. To evaluate the feasibility of the real-time processing design, a series of performance tests have been conducted. The test setup is shown in Fig. 6. In the course of testing, the DU output waveform was captured and stored by an oscilloscope. The waveform data are then converted and fed into an AFG3252 [25] pulse generator to generate the input signal, which is first transferred to a fan-in/out module to fan out eight signals, serving as the input signal of the DAQU. The DAQU output is collected in the CPM and sent to the host PC for analysis.

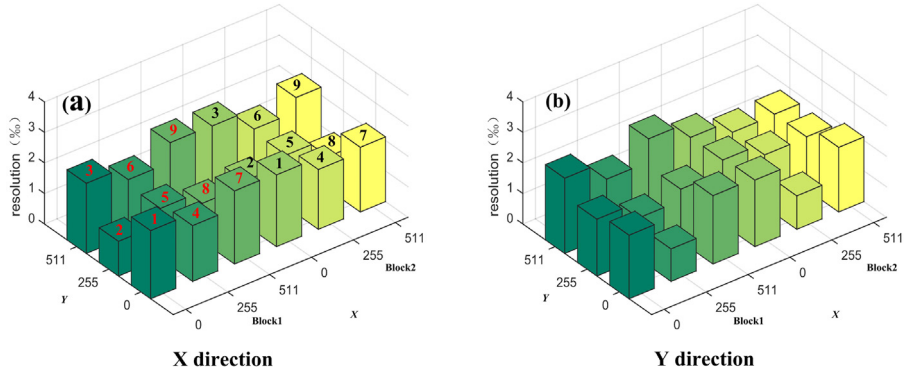

Fig. 8. Position resolution test results of two blocks with one DAQU module. The position number of each block has been superimposed on the picture.

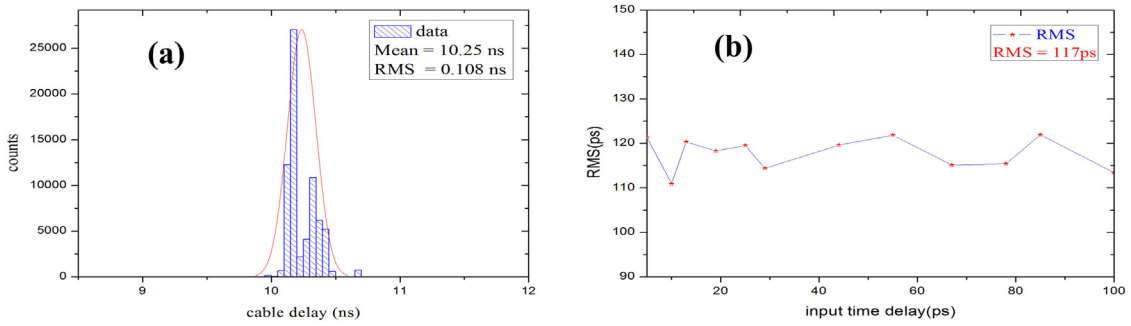

Fig. 9. Time resolution test results for each channel. A typical result with a fixed 10 ns delay time difference between two channels (T_1 and T_2, as described above) on the board.

4.1.1. Position resolution

As aforementioned, see Fig. 4, in the single event processing mode, we first perform position calculation and then used the raw position (X, Y) to find the corresponding crystal bar address, and to make subsequent corrections. Therefore, a test is performed for the calculation of the raw position. The position information was calculated from the 'area' of the 4 analog output signals (marked A, B, C, D) in one detector block, as the formula in (2) and (3). The amplitude ratio among the signals were adjusted and equivalently obtained 9 positions scattered over one detector block covering the center, corners, and edges, to evaluate the DAQU performance.

The bar graph of the nine positions, which represents the x and y directions of one typical detector block in one DU, are given in Fig. 7. The test results of one DAQU board is given in Fig. 8, which indicates that the position resolution of about 2.5‰ RMS was achieved.

4.1.2. Timing resolution

Time resolution is assessed by adopting the cable delay method [17, 26]. The time difference between the two chains changed in the range of 100-ns. Fig. 9(a) shows the typical histogram with a fixed 10 ns delay is obtained 108-ps RMS. In the range of 100-ns delay the time resolution is better than 117-ps RMS, as shown in Fig. 9(b).

4.1.3. Energy resolution

The energy resolution has been experimentally measured for the reference full-scale 650 mV input. Fig. 10 shows the statistical histogram of the energy resolution results of a typical channel (block 1, channel 3) with 650 mV input, from which we can observe that the energy resolution is 1.9 ‰ FWHM [full width half maximum]. Meanwhile, we conducted tests with different input amplitude ranges from 50 to 650 mV for all 8 channels in one DAQU board. The results indicated that the energy resolution is better than 5 ‰, as shown in Fig. 11.

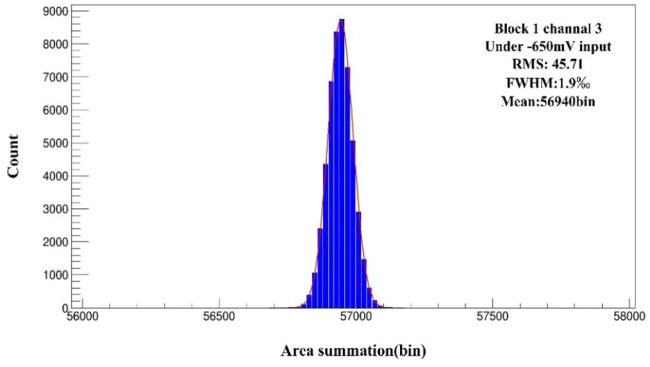

Fig. 10. A statistical histogram of the energy resolution results of a typical channel (Block 1, channel 3) at 650 mV input.

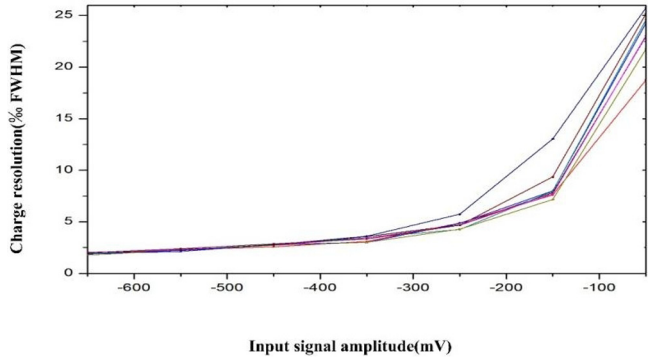

Fig. 11. Tested the resolution of the energy of all channels when the signal amplitude is between 50 mV and 650 mV input. The signal amplitude from the attenuator output ensure that the signal-to-noise ratio of the input signal itself remains unchanged. The energy resolution of all 8 channels on the board with different input signal amplitudes.

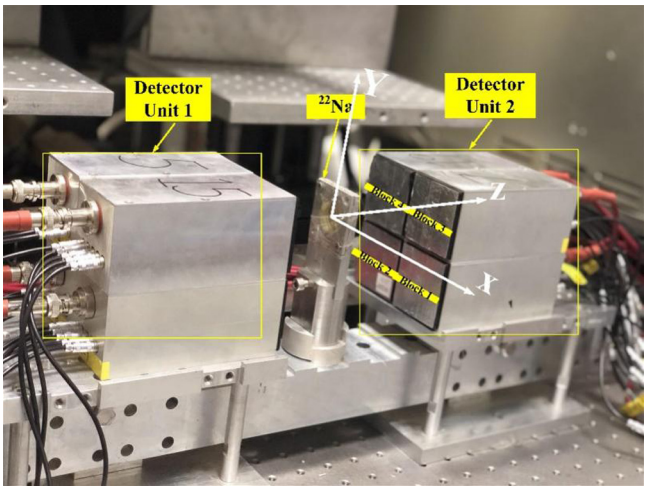

Fig. 12. Installation of the experimental setup in the laboratory. The two detector units and a ^{22}Na source are supported by an anticorodal support.

4.2. Comparison of results for real-time processing and off-line analysis

After the above tests, we further conducted initial commissioning tests with the detectors using ^{22}Na source. Fig. 12 shows the experimental setup of the two detector units, which are mounted at different sides of the ^{22}Na with a distance of 10 cm.

To verify the reliability of the real-time ibPET system, the test results for the single event processing mode [called real-time processing] were compared to that of raw ADC data mode [called off-line analysis]. Due to the randomness of particle detection, the same data sets are used for verification. The obtained data packets not only contain real-time data after hardware processing but also contain the raw data necessary for software processing. The results of crystal identification and photon peak correction can be directly extracted from the real-time data, which were performed by using crystal and normalization lookup tables [called CLUT and NLUT] under self-calibration mode. However, the raw data for crystal identification and photon peak correction are calculated by off-line analysis. The digital processing algorithms for off-line analysis are implemented through computer.

4.2.1. Comparison of crystal identification

The comparison of crystal identification for real-time processing and off-line analysis is shown in Fig. 13(a), which is the 2D position histogram of one LYSO/PMT block. The crystal pixel obtained in real-time processing [red dot] accurately identifies crystals separated by 2.0 mm, which is comparable with the same obtained in the off-line analysis [blue dot]. Although compression can be observed for border crystals, the 20 × 20 crystals are well separated. Moreover, a typical plot of the horizontal and vertical sections of a pixel row is also drawn in (b) and (c), respectively, where the results of the real-time processing and the off-line analysis are represented by red and blue lines. As shown in these plots, the line segments depicted by the two colors are coincident, indicating that the processing results of the real-time and off-line are basically the same. Also we can clearly observe that the horizontal and vertical sections of a pixel list from peak to valley have

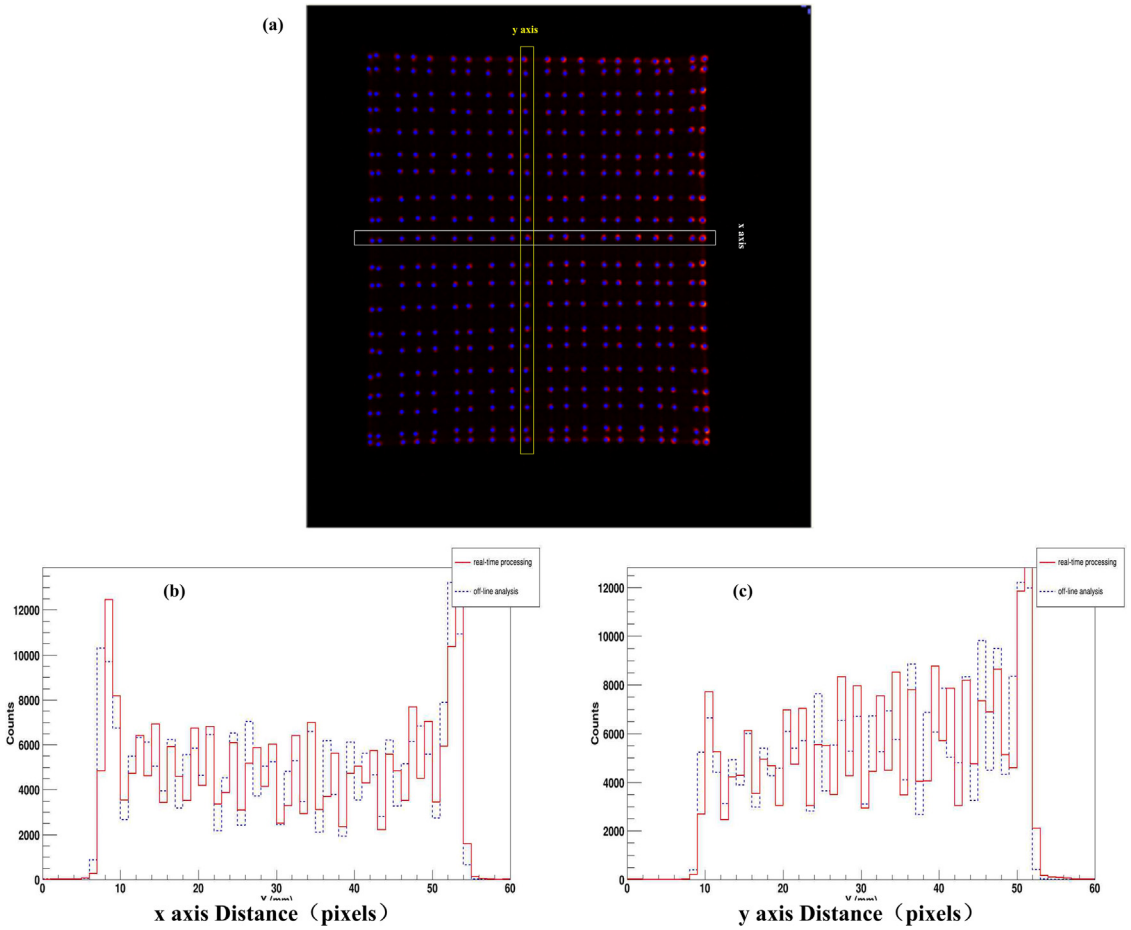

Fig. 13. A typical 2D position histogram of one detector block and 2020 pixels is noticeably visible in (a). Meanwhile, plot of the vertical section of a pixel row and the horizontal section of a pixel list in (b) and (c), respectively.

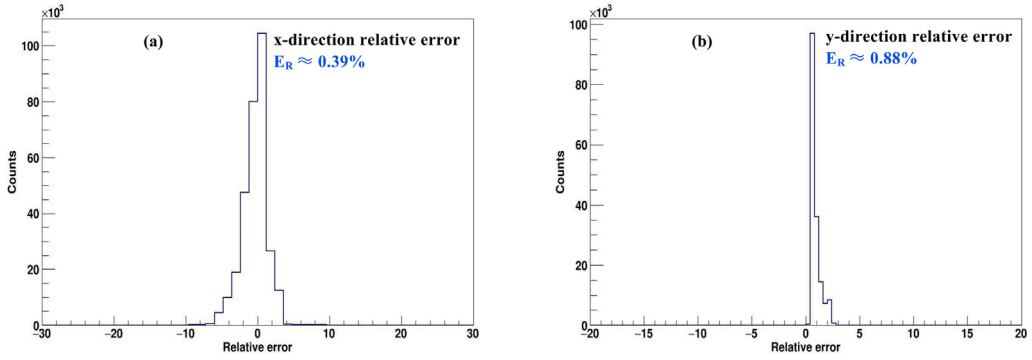

Fig. 14. Relative error (E_R) of the difference between real-time processing and off-line analysis. X-direction E_R (left a) and Y-direction E_R (right b).

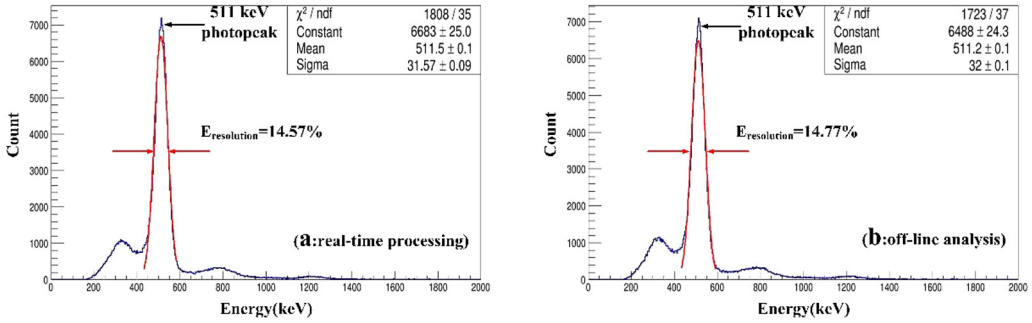

Fig. 15. Photon peak position spectrum of one LYSO/PMT block after applying calibration, where (a) is the result of real-time processing and (b) is the result of off-line analysis.

good separation indicating excellent performance of the real-time logic functions.

Qualitative analysis of the difference between the real-time processing and off-line analysis is conducted, and the reliability of the real-time data processing is demonstrated by the relative error values [ER]. As seen in Fig. 14, the abscissa represents the relative error value [E_R], and the ordinate numbers represents the count value of the corresponding ER. The overall ER of the X- and Y-direction distributions are shown in the figure, which are 0.39% and 0.88%, respectively.

4.2.2. Comparison of photon peak correction

Fig. 15(a) shows the summed energy spectrum for all crystals in one detector module, which is directly extracted from the acquired data of real-time processing. Where, we can observe the photon peak position, which is after correction using the normalization LUT obtained in the self-calibration mode. As shown in Fig. 15(a), the Gaussian fitted photon peak (red curve) shows an overall energy resolution of 14.57% FWHM at 511 keV for the LYSO/PMT block. Conversely, Fig. 15(b) depicts the summed energy spectrum based on the photon-peak position and the energy resolution coefficients, which are both obtained in off-line analysis on the computer. The summed energy spectrum is calibrated to 511 keV for a resolution of 14.77% FWHM. The results indicate that real-time processing is comparable with the same obtained in off-line analysis, proving that meets the online monitoring requirement of the in-beam PET.

5. Conclusion

The design and implementation of FPGA-based real-time digital signal processing and correction is described in this paper. The results of the electronics performance tests indicates that the logic function design works properly. In addition, the comparison of results for real-time processing and off-line analysis indicates that the real-time data processing logic design achieves the online monitoring requirement of the in-beam PET.

Declaration of competing interest

The authors declare that they have no known competing financial interests or personal relationships that could have appeared to influence the work reported in this paper.

Data availability

Data will be made available on request.

Acknowledgments

This work was supported in part by the National Natural Science Foundation of China (No. 11775285), the Science and Technology Research Foundation of Gansu Province (NO. 20JR1RA066), the Youth Innovation Promotion Association, CAS, China (No. 2019408), the Key Deployment Project of Chinese Academy of Sciences (Grant No. KFZD-SW-222) and Fujian Institute of Innovation, CAS (FJCXY18040201).

References

[1] Particle Therapy Co-Operative Group webpage, http://www.ptcog.ch/.
[2] U. Amaldi, G. Kraft, Radiotherapy with beams of carbon ions, Resp. Prog. Phys. 68 (2005) 1861.
[3] D. Schulz-Ertner, H. Tsujii, Particle radiation therapy using proton and heavier ion beams, J. Clin. Oncol. 25 (2007) 953.
[4] P. Crespo, G. Shakirin, et al., Direct time-of-flight for quantitative, real-time in-beam PET: a concept and feasibility study, Phys. Med. Biol. 52 (2007) 6795.
[5] S. Vecchio, et al., A pet prototype for in-beam monitoring of proton therapy, IEEE Trans. Nucl. Sci. 56 (2009) 51.
[6] W. Enghardt, et al., Charged hadron tumour therapy monitoring by means of PET, Nucl. Instrum. Methods A 525 (2004) 284.
[7] T. Nishio, et al., Dose-volume delivery guided proton therapy using beam on-line pet system, Med. Phys. 33 (2006) 51.
[8] C.J. Thompson, Instrumentation for positron emission mammography, PET Clinics 1 (2006) 51.
[9] M.G. Bisogni, et al., INSIDE in-beam positron emission tomography system for particle range monitoring in hadrontherapy, J. Med. Imag. 4 (2017) 011005.

[10] A.C. Kraan, et al., Online monitoring for proton therapy: a real-time procedure using a planar PET system, Nucl. Instrum. Methods A 786 (2015) 120.
[11] J.C. Yang, J. Shi, et al., Design of a compact structure cancer therapy synchrotron, Nucl. Instrum. Methods A 756 (2014) 19.
[12] Demonstration and industrialization of heavy-ion-medical machine (HIMM), Bull. Chin. Acad. Sci. 34 (06) (2019) 722–723.
[13] K. Parodi, et al., PET/CT imaging for treatment verification after proton therapy: A study with plastic phantoms and metallic implants, Med. Phys. 34 (2007) 419.
[14] F. Attanasi, et al., Comparison of two dedicated 'in beam' PET systems via simultaneous imaging of (12)C-induced beta(+)-activity, Phys. Med. Biol. 54 (2) (2009) 29.
[15] X. Niu, J. Yan, et al., Evaluation of energy correction algorithm for signals of PET in Heavy-Ion Cancer Therapy Device, Nucl. Eng. Technol. 52 (1) (2019).
[16] K. Parodi, et al., PET/CT imaging for treatment verification after proton therapy: A study with plastic phantoms and metallic implants, Med. Phys. 34 (2007) 419.
[17] W. Enghardt, et al., Charged hadron tumour therapy monitoring by means of PET, Nucl. Instrum. Methods A 525 (2004) 284.
[18] B.H. Chai, Y. Ji, Lutetium yttrium orthosilicate single crystal scintillator detector. US Patent 920 6, 921, 901. July 26, 2005.
[19] Z. Kuang, et al., Performance of a high-resolution depth encoding PET detector using barium sulfate reflector, Phys. Med. Biol. 62 (2017) 5945.
[20] Hamamatsu Technical Information, H8500 PSPMT, Japan, 2003.
[21] H.R. Qi, et al., Investigation of predigested processing 64 signals of flat-panel PMT, Nucl. Electron. Detect. Technol. 26 (2006) 450.
[22] J.W. Yan, et al., Prototype design of read-out electronics for In-Beam TOF-PET of Heavy-Ion Cancer Therapy Device, Nucl. Instrum. Methods A 959 (2020) 163492.
[23] L.Y. Ke, et al., A design implementation of the central process module for an in-beam PET in HICTD, Nucl. Instrum. Methods A 1013 (2021) 165572.
[24] L.Y. Ke, et al., A real-time sorting algorithm for In-Beam PET of Heavy-Ion cancer Therapy Device, Nucl. Eng. Technol. 52 (2021) 3406–3412.
[25] M. Suda, et al., Medical application of the positron emitter beam at HIMAC, 2000.
[26] L. Zhao, L.-F. Kang, et al., A 16-channel high-resolution time and charge measurement module for the external target experiment in the CSR of HIRFL, Nucl. Sci. Technol. 25 (2014) 10401.